Multimilliwatt, tunable, continuous-wave, mid-infrared generation across 4.6-4.7 μm based on orientation-patterned gallium phosphide

KAVITA DEVI,[1,2,*] A. PADHYE,[1] P. G. SCHUNEMANN,[3] AND M. EBRAHIM-ZADEH[1,4]

[1]ICFO—Institut de Ciencies Fotoniques, The Barcelona Institute of Science and Technology, 08860 Castelldefels (Barcelona), Spain
[2]Department of Physics, Indian Institute of Technology Bhilai, GEC Campus, Sejbahar, Raipur, Chhattisgarh 492015, India
[3]BAE Systems, Inc., MER15-1813, P.O. Box 868, Nashua, New Hampshire 03061-0868, USA
[4]Institucio Catalana de Recerca i Estudis Avancats (ICREA), Passeig Lluis Companys 23, Barcelona 08010, Spain
*Corresponding author: kavita.devi@icfo.eu

Received XX Month XXXX; revised XX Month, XXXX; accepted XX Month XXXX; posted XX Month XXXX (Doc. ID XXXXX); published XX Month XXXX

We report the generation of tunable continuous-wave (cw) mid-infrared (mid-IR) radiation across 4608-4694 nm using the new nonlinear material, orientation-patterned gallium phosphide (OP-GaP). By exploiting difference-frequency-mixing between a cw Tm-fiber laser and a home-built cw optical parametric oscillator in a 40-mm-long crystal, we have generated up to 43 mW of cw output power, with >30 mW across >95% of the mid-IR tuning range. The output at 4608 nm exhibits high beam quality, with a passive power stability of 2.5% rms over 1.5 mins. The temperature acceptance bandwidth of the OP-GaP crystal has been measured and compared with theory. The performance of the mid-IR source at high pump powers and polarization-dependent transmission in OP-GaP has been investigated. © 2018 Optical Society of America

OCIS codes: *(190.2620) Harmonic generation and mixing; (190.4360) Nonlinear optics, devices; (190.4400) Nonlinear optics, materials; (190.4970) Parametric oscillators and amplifiers; (140.3510) Lasers, fiber.*

http://dx.doi.org/10.1364/OL.99.099999

Tunable, continuous-wave (cw) mid-infrared (mid-IR) sources in the difficult spectral range of 4-5 μm are of great interest for many applications such as free-space communication, chemical sensing, and spectroscopy of molecules including CO_2, N_2O and CO, which have characteristic vibrational bands in this region [1]. In this spectral window, quantum cascade lasers represent attractive sources capable of providing Watt-level cw output powers [2-5]. Nonlinear frequency conversion techniques based on difference-frequency generation (DFG) and optical parametric oscillators (OPOs) represent effective alternative approaches for practical generation of widely tunable cw radiation with spectral purity and high beam quality in the mid-IR [6,7]. By exploiting quasi-phase-matched (QPM) nonlinear materials, most notably MgO-doped periodically-poled $LiNbO_3$ (MgO:PPLN), cw OPOs delivering multi-Watt output powers across ~1.5-4 μm have been extensively demonstrated [8]. However, the intrinsic onset of multiphonon absorption in MgO:PPLN and all other oxide-based nonlinear crystals, thermal lensing and dephasing effects, as well as material damage, are fundamental impediments to wavelength generation above ~4 μm. As such, there has been continuous quest for new non-oxide nonlinear materials with wide transparency in mid-IR, while offering attractive linear and nonlinear optical properties for frequency conversion beyond ~4 μm. The most promising nonlinear crystals that have emerged as potential candidates for mid-IR generation beyond ~4 μm include $ZnGeP_2$ (ZGP), $CdSiP_2$ (CSP), orientation-patterned (OP)-GaAs, and OP-GaP [9]. Among these, OP-GaP is the most recently developed QPM semiconductor crystal, which offers wide transparency across ~0.57-12 μm, large optical nonlinearity (d_{14}=70 pm/V) and high thermal conductivity (110 W/m.K). However, cw OPO operation in practical singly-resonant configuration based on OP-GaP or the other non-oxide crystals remains challenging, due to the intrinsically high threshold powers under low cw pumping intensities, which in turn requires high-quality and low-loss crystals, mirrors, and crystal coatings.

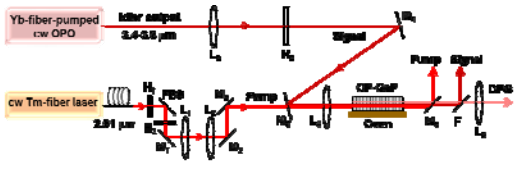

Fig. 1. Schematic of the experimental setup. PBS: polarizing beam splitter; H_{1-3}: half-wave plates; L_{1-5}: lenses; M_{1-6}: mirrors; F: filter.

On the other hand, the DFG approach which is single-pass and does not require the attainment of an oscillation threshold,

currently offers an attractive alternative for mid-IR generation [10]. By exploiting OP-GaP, cw DFG has recently been explored at fixed wavelengths of 3.4 μm [11] and at 5.85 μm [12]. However, given the significance of the 4-5 μm spectral window and the recent development of OP-GaP as a promising new mid-IR nonlinear material, it is important to study tunable wavelength generation in this crystal. Here we report, for the first time to our knowledge, the generation of tunable cw radiation across 4608-4694 nm based on DFG in OP-GaP. We have achieved practical mid-IR output powers of >30 mW across 96% of the DFG tuning range, with up to 43 mW at 4608 nm and 4635 nm, in high spatial beam quality.

The schematic of the experimental setup is shown in Fig. 1. The pump source is a commercial cw Tm-fiber laser (IPG Photonics, TLR-50-2010-LP), delivering up to 40 W of output power at 2.010 μm in a linearly polarized beam. The laser is operated at maximum power, and the input power for DFG is adjusted using a combination of a half-wave plate (H_1) and a polarizing beam-splitter (PBS). A second half-wave plate (H_2) is used to control the pump polarization for phase-matching in the DFG crystal. The lenses, $L_{1,2}$, are used to adjust the Tm-fiber pump beam diameter. The input signal for DFG is the idler output beam derived from a home-built cw OPO based on a 38-mm-long MgO:PPLN crystal with a single grating period, Λ_{OPO}=30 μm, pumped by a commercial cw Yb-fiber laser (IPG Photonics, YLR-30-1064-LP-SF) at 1.064 μm. The SRO provides up to ~2.5 W of tunable cw output power in the non-resonant idler beam across 3.37–3.62 μm. The OPO idler output power is adjusted by varying the Yb-fiber pump power. A lens, L_3, is used to collimate the DFG input signal, namely the OPO idler beam, and a tunable uncoated MgF_2 half-wave plate (H_3) is used to control the incident signal polarization for phase-matching in the DFG process. The tilt angle of H_3 is adjusted for optimum performance at any given signal wavelength. Plane mirror, M_1, is used to steer the Tm-fiber pump beam, while two pairs of plane mirrors, $M_{2,3}$ and $M_{4,5}$, are used to optimize the spatial overlap of the Tm-fiber pump beam and input signal beam on lens, L_4, respectively. The mirror, M_5, is highly transmitting (T>99%) for the pump (at 2.010 μm), while reflective (R>90%) for the input signal (over 3.37–3.62 μm). The nonlinear crystal used for DFG is

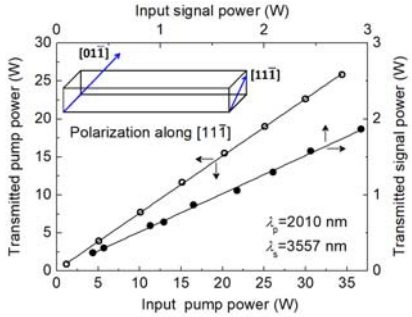

Fig. 2. Transmission of the 40-mm-long OP-GaP sample at 2010 nm and 3557 nm. Inset: Polarization directions along crystal axes.

40-mm-long OP-GaP with a grating period of Λ_{DFG}=85.1 μm. The crystal has a physical aperture, 6-mm-wide, and 1.7-mm-thick, and has antireflection (AR)-coated end-faces (R<1%) over 1.98-2.1 μm, 3.3-3.75 μm, and 4.45-4.8 μm. It is housed in an oven with stability of ±0.1°C, which can be controlled from room temperature to 200°C. The lens, L_4, of focal length, f=300 mm, is used to focus the pump and signal beam to waist radii of w_{0p}~52 μm and w_{0s}~80 μm, corresponding to confocal focusing parameters of ξ_p=1.5 and ξ_s=1.3, respectively, at the center of the OP-GaP crystal. Dichroic mirror, M_6, is used to separate pump, while filter F is used to separate the signal, from the output DFG beam. A lens, L_5, is used to collimate the DFG output beam.

We initially investigated polarization-dependent transmission characteristics of the OP-GaP crystal by varying the polarization of the input pump and signal beams using H_2 and H_3, respectively. We first performed the transmission measurements by keeping the polarization of both input beams along the [11$\bar{1}$] direction in the crystal, for which maximum DFG power in OP-GaP has been generated. The results, obtained at wavelengths 2010 nm and 3557 nm, are shown in Fig. 2. The different polarization directions along the OP-GaP crystal axes are shown in the inset of Fig. 2. The polarization direction [11$\bar{1}$] lies on the incident face of the crystal and is perpendicular to the propagation direction. As can be seen in Fig. 2, the transmitted power has linear dependence on the input pump powers, with a transmission of 75.1% and 62.7% at λ_p=2010 nm and λ_s=3557 nm, respectively. By changing the pump polarization to [01$\bar{1}$] direction and signal polarization to any arbitrary direction, the DFG efficiency was observed to decrease by ~40%. Under this condition, however, the transmission for the pump beam along [01$\bar{1}$] direction was measured to be 76.5%. The lower transmission measured at any polarization in the present OP-GaP could be due to the absorption at these wavelengths, which may be the result of possible diffusion of impurities from the GaP substrate wafer into the hydride vapor phase epitaxy (HVPE)-grown QPM layer or due to the silicon impurities originated during fabrication.

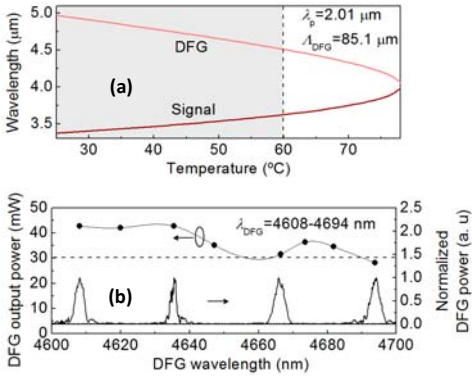

Fig. 3. (a) Theoretical temperature tuning curve using OP-GaP with Λ_{DFG}=85.1 μm, pumped at 2.01 μm. Curve across shaded region shows the output DFG and input signal wavelength range using MgO:PPLN with Λ_{OPO}=30 μm. (b) Variation of DFG power and DFG output spectra across the tuning range, at maximum pump and signal powers.

We then studied the spectral tuning characteristics of the DFG output in the mid-IR by tuning the input signal, namely the OPO idler wavelength. By varying the MgO:PPLN crystal temperature, T_{OPO}, over 80-115 ºC, resulting in an OPO idler tuning across 3505-3557 nm, and simultaneously adjusting the phase-matching temperature of the OP-GaP crystal, T_{DFG}, over 25-31.8 ºC, we were

able to tune the DFG output across 4608-4694 nm. The phase-matching temperature of the crystals, T_{OPO} and T_{DFG}, recorded in the present work are the temperature of the oven. It is to be noted that for a fixed pump wavelength at 2.010 μm and an OP-GaP grating period of Λ_{DFG}=85.1 μm, by tuning the input signal over 3.37-3.98 μm and simultaneously varying T_{DFG} over 25-78 ºC, a theoretically calculated DFG tuning range across 4.05-4.97 μm can be obtained. This is shown in Fig. 3(a), where the theoretical temperature tuning curve is calculated using the relevant Sellmeier equations for OP-GaP [13]. In the present work, however, with the single grating period of Λ_{OPO}=30 μm in the MgO:PPLN crystal, the DFG input signal (OPO output idler) can be tuned across 3.37–3.62 μm, shown as shaded region in Fig. 3(a), resulting in a theoretical DFG tuning range across 4.51-4.97 μm. At the same time, in our experiment, the generation of DFG wavelengths above 4694 nm was limited by the oven, requiring temperatures below 25ºC. Also, given the low output powers at longer OPO idler wavelengths with the current MgO:PPLN crystal, we performed the DFG spectral tuning down to 4608 nm.

While maintaining the polarizations along [11$\bar{1}$] direction, we measured the DFG output power across the tuning range for the maximum available Tm-fiber input pump power at 34 W, and a maximum input signal power of ~3 W at any wavelength, while also maintaining the optimum polarization for both beams into the OP-GaP crystal. The results are shown in Fig. 3(b). As evident, the DFG output power reaches a maximum of 43 mW at 4608 nm and 4635 nm, providing >40 mW over 37% and and >30 mW over 96% of the full tuning range. Also shown in Fig. 3(b) are the DFG spectra across the tuning range, measured using a spectrum analyser (Bristol 721), with a spectral resolution of 6 GHz in the mid-IR. As can be seen, the spectrum at all wavelengths has a full-width at half-maximum (FWHM) linewidth of ~3 nm (~42 GHz). Although the input signal (OPO idler) beam is single-frequency, the finite linewidth of the output DFG spectrum could be attributed to the finite Tm-fiber pump laser bandwidth of ~0.7 nm.

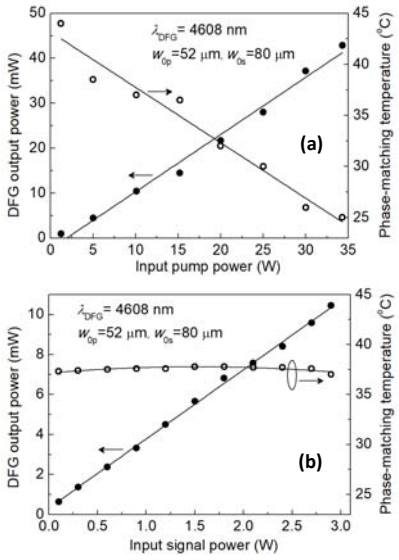

Fig. 4. Dependence of the measured cw DFG power and OP-GaP phase-matching temperature on (a) incident pump power, and (b) incident signal power. Solid lines are guide to the eye.

To study the power scaling capability of the source, we recorded the variation of DFG output power with the incident Tm-fiber pump and signal power, while keeping either of the input powers fixed. Figure 4(a) shows the DFG output power at 4608 nm as a function of pump power, with the input signal power fixed at 2.9 W. The DFG power increases linearly with pump power, reaching 43 mW for 34 W of input power. To generate the maximum DFG power, the OP-GaP crystal temperature was optimized at each pump power level. Also shown in Fig. 4(a) is the change in the DFG phase-matching temperature of the OP-GaP crystal, T_{DFG}, with increase in pump power, where a drop from 44 ºC to 25 ºC is recorded as the Tm-fiber pump power is increased from 1.2 W to 34 W. This implies the heating of the crystal at high input pump powers, which is attributed to significant absorption in the OP-GaP sample. We then recorded the DFG output power at 4608 nm as a function of input signal power, together with the corresponding variation in the phase-matching temperature of the OP-GaP crystal, while keeping the Tm-fiber pump power fixed. The results are shown in Fig. 4(b). To minimize the constant heating of the crystal at high pump power, we limited the pump power to 10 W and varied the input signal power up to the maximum of 2.9 W. The DFG power is seen to increase linearly with input signal power, but the phase-matching temperature, T_{DFG}, is observed to remain constant with the increase in signal power. This is to be expected, given that both the pump power and the maximum input signal power are relatively low, resulting in negligible heating in the OP-GaP crystal, despite significant absorption. At the same time, we also observed a change in the wavelength of the DFG input signal (OPO idler) with the increase in Yb-fiber pump power to the OPO. The signal wavelength was measured to decrease by ~5 nm as the signal power was increased from 1 W to 2.9 W. Hence, for the attainment of optimum phase-matching for DFG, the temperature of the OP-GaP crystal had to be increased by ~0.6 ºC with the increase in signal power. This temperature rise was balanced by the cooling of the crystal to compensate for the heating effect at higher signal powers. We also investigated tighter and looser focusing for both pump and signal beams, with smaller beam waist radii, w_{0p}~47.5 μm (ξ_{0p}~1.8), w_{0s}~69 μm (ξ_{0s}~1.7), and larger beam waist radii, w_{0p}~97 μm (ξ_{0p}~0.4), w_{0s}~130 μm (ξ_{0s}~0.5) at the center of the OP-GaP crystal, by changing the focal length of lens, L_4. This resulted in lower DFG output power, which we attribute to reduced spatial overlap of pump and signal beams within the OP-GaP crystal.

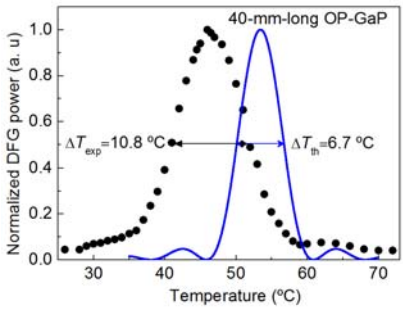

Fig. 5. Experimentally measured (solid circle), and theoretically calculated (solid line) temperature acceptance bandwidth of DFG output for 40-mm-long OP-GaP.

We further performed temperature acceptance bandwidth measurements for DFG at 4608 nm in the 40-mm-long OP-GaP crystal. To minimize thermal contributions, the measurements were performed at an input Tm-fiber pump power of 5 W and signal power of 1 W, with loose focussing (w_{0p}~97 μm, w_{0s}~130 μm). The temperature acceptance bandwidth was determined by measuring the variation of DFG output power as a function of the phase-matching temperature, with the result shown in Fig. 5. As can be seen, the experimental data result in a FWHM temperature acceptance bandwidth of ΔT_{exp}=10.8 ºC at T_{DFG}=46 ºC. Also shown in Fig. 5 is the theoretical temperature acceptance curve calculated for single-frequency input beams in plane-wave approximation without focusing, using the relevant Sellmeier equations for OP-GaP [13], where a FWHM bandwidth of ΔT_{th}=6.7 ºC at a phase-matching temperature of T_{th}=53.4 ºC is obtained. The discrepancy between the experimental and theoretical value of temperature acceptance bandwidth could be in part due to the finite bandwidth of the Tm-fiber pump laser ($\Delta\lambda_p$~0.7 nm) and the plane-wave approximation in theoretical calculation, while the discrepancy in the value of phase-matching temperature under minimum thermal contribution could be due to possible non-uniformity in the grating period along the 40-mm-long OP-GaP crystal sample as well as the non-negligible absorption in the OP-GaP crystal.

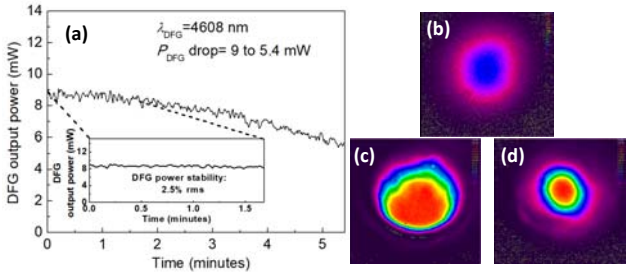

Fig. 6. (a) DFG output passive power stability under free running condition over more than 5 mins. Inset: Zoomed version of DFG output passive power stability over initial 1 min 40 secs. Far-field energy distribution of the (b) DFG output beam, (c) input signal beam, and (d) input pump beam.

We also recorded the passive power stability of the DFG output at 4608 nm at an input Tm-fiber pump power of 10 W and signal power of 2.6 W, under free-running conditions. The result is shown in Fig. 6(a). As seen, the generated power decreases from 9 mW to 5.4 mW over 5 mins at fixed input powers with a rise in crystal temperature from 38 ºC to 42.5 ºC. The drop in the output power is attributed to the change in phase matching temperature. The generated DFG power exhibits a passive stability better than 2.5% rms over the initial 1 min 40 secs time duration, before the onset of rise in crystal temperature, as shown in the inset of Fig. 6(a). The instability in power over this time duration could be due to mechanical vibrations and air currents in the laboratory and possible mode-hopping in the OPO idler in the absence of active stabilization. We have not observed any damage to the crystal or AR coatings after long-term operation. The far-field energy distribution of the DFG output at 4608 nm, at maximum pump and signal power, for the collimated beam was also recorded using Pyrocam III camera, as shown in Fig. 6(b). The result confirms excellent spatial quality with a beam circularity >92%. Similar profiles were obtained across the entire DFG tuning range. Figure 6(c) and 6(d) shows the far-field energy distribution for the input signal and pump beams, where circularity of >93% and >97%, respectively, has been measured. As evident, the beam quality has been transferred from the input pump and signal to the DFG output and no degradation in the DFG beam profile has been observed at maximum pump powers. Further, throughout our experiments, we did not observe any variation in the spatial mode of the input and output pump and signal beams, indicating the absence of thermal lensing in the crystal.

In conclusion, we have demonstrated the generation of tunable cw mid-IR radiation across 4608-4694 nm in OP-GaP, for the first time to our knowledge. By exploiting single-pass DFG between a cw Tm-fiber laser and a cw OPO, we have generated up to 43 mW of mid-IR cw power with >30 mW across 96% of the tuning range in excellent spatial beam quality. The absence of saturation in DFG output power at higher pump powers suggests the possibility of further scaling of DFG power with increase in pump power and improved crystal quality. Using OP-GaP with slightly longer grating period of Λ_{DFG}=87 μm, the DFG spectral tuning can be further extended up to 5000 nm with high output powers, using the same Tm-fiber laser at 2.01 μm, and signal (OPO idler) wavelengths across 3.37-3.51 μm. The results demonstrate the potential of OP-GaP for tunable mid-IR generation across the difficult 4-5 μm spectral range, of interest for many applications.

Funding. Ministerio de Economía y Competitividad (MINECO) (NuOPO, TEC2015-68234-R); European Commission (EC) (Mid-Tech, H2020-MSCA-ITN-2014); Generalitat de Catalunya (CERCA Programme); Severo Ochoa Programme for Centres of Excellence in R&D (SEV-2015-0522); Fundación Cellex.

References

1. M. Ebrahim-Zadeh and I. T. Sorokina, eds., Mid-Infrared Coherent Sources and Applications (Springer, 2008), pp. 347–375.
2. R. Maulini, I. Dunayevskiy, A. Lyakh, A. Tsekoun, C.K.N. Patel, L. Diehl, C. Pflugl and F. Capasso, Elect. Lett., 45, 107-108 (2009).
3. F. Capasso, Opt. Eng. 49, 111102 (2010).
4. Y. Bai, N. Bandyopadhyay, S. Tsao, S. Slivken, and M. Razeghi, Appl. Phys. Lett. **98**, 181102 (2011).
5. S. Slivken, S. Sengupta, and M. Razeghi, Appl. Phys. Lett. **107**, 251101 (2015).
6. W. Chen, J. Cousin, E. Poullet, J. Burie, D. Boucher, X. Gao, M. W. Sigrist, and F. K. Tittel, C.R. Physique **8**, 1129 (2007).
7. M. Ebrahim-Zadeh, "Continuous-wave optical parametric oscillators," in *Handbook of Optics* (OSA, vol IV, 2010), Chap. 17.
8. M. Ebrahim-Zadeh, S. Chaitanya Kumar, and K. Devi, IEEE J. Sel. Top. Quantum Electron. **20**, 0902823 (2014).
9. P. G. Schunemann, K. T. Zawilski, L. A. Pomeranz, D. J. Creeden, and P. A. Budni, J. Opt. Soc. Am. B **33**, D36 (2016).
10. K. Devi, P. G. Schunemann, and M. Ebrahim-Zadeh, Opt. Lett. **39**, 6751 (2014).
11. S. Guha, J. O. Barnes and P. G. Schunemann, Opt. Mater. Express **5**, 2911 (2015).
12. G. Insero, C. Clivati, D. D'Ambrosio, P. D. Natale, G. Santambrogio, P. G. Schunemann, J. J. Zondy, and S. Borri, Opt. Lett. **41**, 5114 (2016).
13. P. G. Schunemann, L. A. Pomeranz, D. J. Magarrell, J. C. McCarthy, K. T. Zawilski, D. E. Zelmon, *CLEO USA, OSA Technical Digest (online)*, paper SW3O.4 (2015).

References with title

1. M. Ebrahim-Zadeh and I. T. Sorokina, eds., Mid-Infrared Coherent Sources and Applications (Springer, 2008), pp. 347–375.
2. R. Maulini, I. Dunayevskiy, A. Lyakh, A. Tsekoun, C.K.N. Patel, L. Diehl, C. Pflugl and F. Capasso, "Widely tunable high-power external cavity quantum cascade laser operating in continuous-wave at room temperature," Elect. Lett., 45, 107-108 (2009).
3. F. Capasso, "High-performance mid infrared quantum cascade lasers," Opt. Eng. 49, 111102 (2010).
4. Y. Bai, N. Bandyopadhyay, S. Tsao, S. Slivken, and M. Razeghi, "Room temperature quantum cascade lasers with 27% wall plug efficiency," Appl. Phys. Lett. **98**, 181102 (2011).
5. S. Slivken, S. Sengupta, and M. Razeghi, "High power continuous operation of a widely tunable quantum cascade laser with an integrated amplifier," Appl. Phys. Lett. **107**, 251101 (2015).
6. W. Chen, J. Cousin, E. Poullet, J. Burie, D. Boucher, X. Gao, M. W. Sigrist, and F. K. Tittel, "Continuous-wave mid-infrared laser sources based on difference frequency generation," C.R. Physique **8**, 1129-1150 (2007).
7. M. Ebrahim-Zadeh, "Continuous-wave optical parametric oscillators," in *Handbook of Optics* (OSA, vol IV, 2010), Chap. 17.
8. M. Ebrahim-Zadeh, S. Chaitanya Kumar, and K. Devi, "Yb-fiber-laser-pumped continuous-wave frequency conversion sources from the mid-infrared to the ultraviolet," IEEE J. Sel. Top. Quantum Electron. **20**, 0902823 (2014).
9. P. G. Schunemann, K. T. Zawilski, L. A. Pomeranz, D. J. Creeden, and P. A. Budni, "Advances in nonlinear optical crystals for mid-infrared coherent sources," J. Opt. Soc. Am. B **33**, D36-D43 (2016).
10. K. Devi, P. G. Schunemann, and M. Ebrahim-Zadeh, "Continuous-wave, multimilliwatt, mid-infrared source tunable across 6.4–7.5 μm based on orientation-patterned GaAs," Opt. Lett. **39**, 6751-6754 (2014).
11. S. Guha, J. O. Barnes and P. G. Schunemann, "Mid-wave infrared generation by difference frequency mixing of continuous wave lasers in orientation-patterned Gallium Phosphide," Opt. Mater. Express **5**, 2911-2923 (2015).
12. G. Insero, C. Clivati, D. D'Ambrosio, P. D. Natale, G. Santambrogio, P. G. Schunemann, J. J. Zondy, and S. Borri, "Difference frequency generation in the mid-infrared with orientation-patterned gallium phosphide crystals," Opt. Lett. **41**, 5114-5117 (2016).
13. P. G. Schunemann, L. A. Pomeranz, D. J. Magarrell, J. C. McCarthy, K. T. Zawilski, D. E. Zelmon, "1064-nm-pumped mid-infrared optical parametric oscillator based on orientation-patterned gallium phosphide (OP-GaP)," *CLEO USA, OSA Technical Digest (online)*, paper SW3O.4 (2015).